Original Article

MOLECULAR METABOLISM

Sodium salicylate rewires hepatic metabolic pathways in obesity and attenuates IL-1β secretion from adipose tissue: The implications for obesity-impaired reverse cholesterol transport

Sarina Kajani [1,2,3,5], Sean Curley [1,2,3,5], Marcella E. O'Reilly [1,2,3,5], Xiaofei Yin [3,5,7], Eugene T. Dillon [6], Weili Guo [1,2,3,5], Kanishka N. Nilaweera [8,9], Lorraine Brennan [3,5,7], Helen M. Roche [1,3,4,5], Fiona C. McGillicuddy [1,2,3,5,*]

ABSTRACT

Introduction: High-fat diet (HFD)-induced obesity impairs clearance of cholesterol through the Reverse Cholesterol Transport (RCT) pathway, with downregulation in hepatic expression of cholesterol and bile acid transporters, namely ABCG5/8 and ABCB11, and reduced high-density lipoprotein (HDL) cholesterol efflux capacity (CEC). In the current study, we hypothesized that the development of hepatosteatosis, secondary to adipose-tissue dysfunction, contributes to obesity-impaired RCT and that such effects could be mitigated using the anti-inflammatory drug sodium salicylate (NaS).

Materials and methods: C57BL/6J mice, fed HFD ± NaS or low-fat diet (LFD) for 24 weeks, underwent glucose and insulin tolerance testing. The ^{3}H-cholesterol movement from macrophage-to-feces was assessed *in vivo*. HDL-CEC was determined *ex vivo*. Cytokine secretion from adipose-derived stromal vascular fraction (SVF) cells was measured *ex vivo*. Liver and HDL proteins were determined by mass spectrometry and analyzed using Ingenuity Pathway Analysis.

Results: NaS delayed HFD-induced weight gain, abrogated priming of pro-IL-1β in SVFs, attenuated insulin resistance, and prevented steatohepatitis (ectopic fat accumulation in the liver). Prevention of hepatosteatosis coincided with increased expression of PPAR-alpha/beta-oxidation proteins with NaS and reduced expression of LXR/RXR-induced proteins including apolipoproteins. The latter effects were mirrored within the HDL proteome in circulation. Despite remarkable protection shown against steatosis, HFD-induced hypercholesterolemia and repression of the liver-to-bile cholesterol transporter, ABCG5/8, could not be rescued with NaS.

Discussions and conclusions: The cardiometabolic health benefits of NaS may be attributed to the reprogramming of hepatic metabolic pathways to increase fatty acid utilization in the settings of nutritional overabundance. Reduced hepatic cholesterol levels, coupled with reduced LXR/RXR-induced proteins, may underlie the lack of rescue of ABCG5/8 expression with NaS. This remarkable protection against HFD-induced hepatosteatosis did not translate to improvements in cholesterol homeostasis.

Keywords Metabolic inflammation; Reverse cholesterol transport; Liver proteomics; Sodium salicylate; HDL proteomics; Hepatosteatosis

1. INTRODUCTION

Obesity is a complex multifactorial disease, with a chronic inflammatory underpinning [1] and is associated with numerous complications including insulin resistance that often co-present [2,3] non-alcoholic fatty liver disease (NAFLD), non-alcoholic steatohepatitis (NASH) [4], and hypercholesterolemia and cardiovascular disease (CVD) [5]. Reverse cholesterol transport (RCT) is the atheroprotective process by which cholesterol within peripheral cells is effluxed onto high-density lipoprotein (HDL) particles and returned to the liver for excretion in bile and feces [6], perturbations in RCT can cause cholesterol retention *in vivo* and enhance CVD risk [7,8]. We have

[1]Diabetes Complications Research Centre, Ireland [2]UCD School of Medicine, Ireland [3]UCD Conway Institute, Ireland [4]Nutrigenomics Research Group, School of Public Health, Physiotherapy and Sports Science, Ireland [5]UCD Institute of Food and Health, Ireland [6]Mass Spectrometry Resource, Ireland [7]School of Agriculture and Food Science, University College Dublin, Dublin 4, Ireland [8]Teagasc Food Research Centre, Ireland [9]VistaMilk Research Centre, Moorepark, Fermoy, Ireland

*Corresponding author. UCD School of Medicine, UCD Conway Institute, Belfield, Dublin 4, Ireland. E-mail: fiona.mcgillicuddy@ucd.ie (F.C. McGillicuddy).

Abbreviations: HFD, High-fat diet; IPA, Ingenuity Pathway Analysis; RCT, Reverse Cholesterol Transport; ABCA1, ATP binding cassette (ABC) transporter subfamily A, member 1; ABCG5/8, ATP binding cassette (ABC) transporter subfamily G, member 5/8; ABCB11, ATP binding cassette (ABC) transporter subfamily B member 11; HDL, High-density lipoprotein; cAMP, cyclic adenosine monophosphate; LXR, liver-X-receptor; PPAR, peroxisome proliferator-activator receptor; RXR, retinoid-X-receptor

Received September 30, 2021 • Revision received December 13, 2021 • Accepted December 21, 2021 • Available online 24 December 2021

https://doi.org/10.1016/j.molmet.2021.101425

previously demonstrated that high-fat diet (HFD)-induced obesity in C57BL/6J mice impairs HDL cholesterol efflux capacity (CEC) and impedes liver-to-feces RCT with reduced expression of free cholesterol [ATP binding cassette (ABC) transporter subfamily G, member 5/8, (ABCG5/8)] and bile-acid [ATP binding cassette (ABC) transporter subfamily G, member 11 (ABCB11)] transporters in the livers relative to low-fat diet (LFD) control [9]. Furthermore, the HDL proteome was enriched with pro-inflammatory liver-derived proteins and was depleted of anti-oxidant/anti-inflammatory proteins in obese mice consuming a saturated fatty acid (SFA)-enriched HFD, relative to obese mice consuming a monounsaturated fatty acid (MUFA)-enriched HFD, coincident with greater hepatic inflammation after SFA-HFD [9]. Acute inflammation similarly reduces HDL-CEC in mice [10] and humans [11] and liver-to-feces RCT [10] prompting us to hypothesize that a) obesity-induced metabolic inflammation underpins impaired RCT and b) anti-inflammatory intervention would rescue obesity-impaired RCT. Therapeutically targeting the RCT pathway in patients with obesity may offer an important stratified approach to combatting excessive risk of cardiovascular disease (CVD) within this population.

Adipose-tissue inflammation and subsequent loss of functionality are thought to be key drivers of ectopic fat deposition in secondary organs including the liver during obesity [12]. Adipose-tissue inflammation occurs in a time-dependent manner with initial recruitment of T-cells (~6w) followed by monocytes/macrophages (10–12w) [13]. Endogenous danger signals including cholesterol and SFA [14–17] typify obesity, prime pro-IL-1β production within immune cell populations contributing to the development of insulin resistance [14].

Sodium salicylate (NaS), a pleiotropic drug, is well known for its beneficial effects on glucose metabolism [18–20]; it inhibits NFκB [21], IκB kinase beta (IKKβ) [22] and cyclooxygenase 2 (COX2) [23–25]. Activation of the metabolic sensor adenosine monophosphate kinase (AMPK) [26] and enhanced activation of brown adipose tissue [27] have also been purported to be the critical mediators of the beneficial effects of salicylate on metabolism. In this study, we hypothesized that NaS intervention would attenuate HFD-induced adipose tissue and liver inflammation, protect against hepatosteatosis, thereby preserving efficient cholesterol trafficking through the liver to feces.

Within this study, we utilized obesity-prone C57BL/6J mice to track ^{3}H-cholesterol movement from injected macrophage-to-feces [28] after both short-term (4w) (prior to metabolic inflammation) and long-term (24w) (significant metabolic inflammation) exposure to an obesogenic HFD supplemented ± NaS. This mouse model reflects human physiology with significant induction of adipose inflammation, hyperinsulinemia, insulin resistance, and hepatosteatosis after high-fat feeding over time. Our study design allowed us to decipher a) whether short-term exposure to HFD (4w), prior to significant adipose tissue inflammation, impacts RCT and b) whether reduced metabolic inflammation in response to NaS, after long-term exposure to HFD (24w), rescues obesity-impaired RCT.

2. MATERIALS & METHODS

2.1. Materials

Cholesterol [1,2–3H(N)] was purchased from Perkin–Elmer Analytical Sciences (Ireland). Cell culture material was purchased from Lonza (Slough, UK). All other reagents, unless otherwise stated, were obtained from Sigma Aldrich Ltd.

2.2. Animals

Animal care, procedures, and ethical approval were obtained from UCD, Ireland and UCC Ethics Committee. The mice were maintained according to the provisions of the European Union (Directive 2010/63/EU) and the Republic of Ireland guidelines (SI No 543 of 2012). Male C57BL/6J (6–8 weeks old, Harlan Laboratories, UK) were randomized into cages (n = 4/cage) and housed using 12 h dark/light cycles provided with water and fed *ad libitum.* Cages were randomized to HFD (60% kCal from soybean oil and lard), HFD + NaS (6 g/kg NaS in diet), or a micronutrient-matched LFD (10% kCal from soybean oil and lard) (Research Diets, Inc., New Brunswick, NJ, USA) for up to 24w ($n = 16$ experimental animals per group, $n = 4$ separate cages per group). Bodyweight and food consumption were measured weekly.

2.3. Rodent *in vivo* RCT studies

Labeled J774.2 macrophages (European Collection of Cell Cultures) (~2×10^6 cells/4×10^6 dpm/mouse) were injected into C57BL/6J mice in the intraperitoneal cavity; the mice were housed individually in metabolic cages (Tecniplast, PA, USA) from 12 to 24 h post-injection and fed respective diets *ad libitum*. Cells were mycoplasma tested and IMPACT (IDEXX Laboratories, Inc., Maine, USA)-tested prior to injection. Blood samples were taken via the retro-orbital plexus under anesthesia at 4, 24, and 48 h. After 48 h, the mice were euthanized by cervical dislocation. Adipose, liver, and feces were isolated and prepared for lipid, protein, and mRNA analyses as described and in the supplement. ^{3}H-label counts were measured by liquid scintillation counting (LSC). No adverse effects were noticed.

2.4. Labeling of macrophage for RCT studies and cholesterol efflux assays

RCT: J774.2 macrophages were incubated for 48 h in labeling media containing acetylated-LDL (25 μg/mL) (Intracel, USA) and ^{3}H-cholesterol (5 μCi/mL). The cells were washed, equilibrated, centrifuged, and re-suspended in minimal essential media (MEM) prior to intraperitoneal injection.

2.5. Cholesterol efflux assay

J774.2 macrophages were labelled for 24 h with ^{3}H-cholesterol (1 μCi/mL) and equilibrated overnight in 0.2% bovine serum albumin (BSA) ± cAMP (0.3 mM) to drive ABCA1 expression. ApoB-containing lipoproteins were removed from mouse plasma by polyethylene glycol (PEG) precipitation. *Ex vivo* efflux from labeled macrophages to 2.8% HDL supernatant or MEM background control was measured over 4 h. The difference in efflux from cells stimulated in the presence or absence of cAMP represents ABCA1-dependent efflux. ABCA1-independent efflux was derived from untreated (-cAMP) cells.

2.6. Proteomics

Hepatic protein (100 μg) and HDL particles (fraction 36–38, separated by fast protein liquid chromatography (FPLC)) underwent overnight in-solution trypsin digestion and were processed for mass spectrometry (see supplementary material). Peptide fractions were analyzed on a quadrupole Orbitrap mass spectrometer equipped with a reversed-phase NanoLC UltiMate 3000 HPLC system (Thermo Fisher Scientific, Inc.). Peptides and proteins were matched to the UniProt Human database and label-free quantitative (LFQ) ion intensities were generated using the default setting of MaxQuant, a quantitative

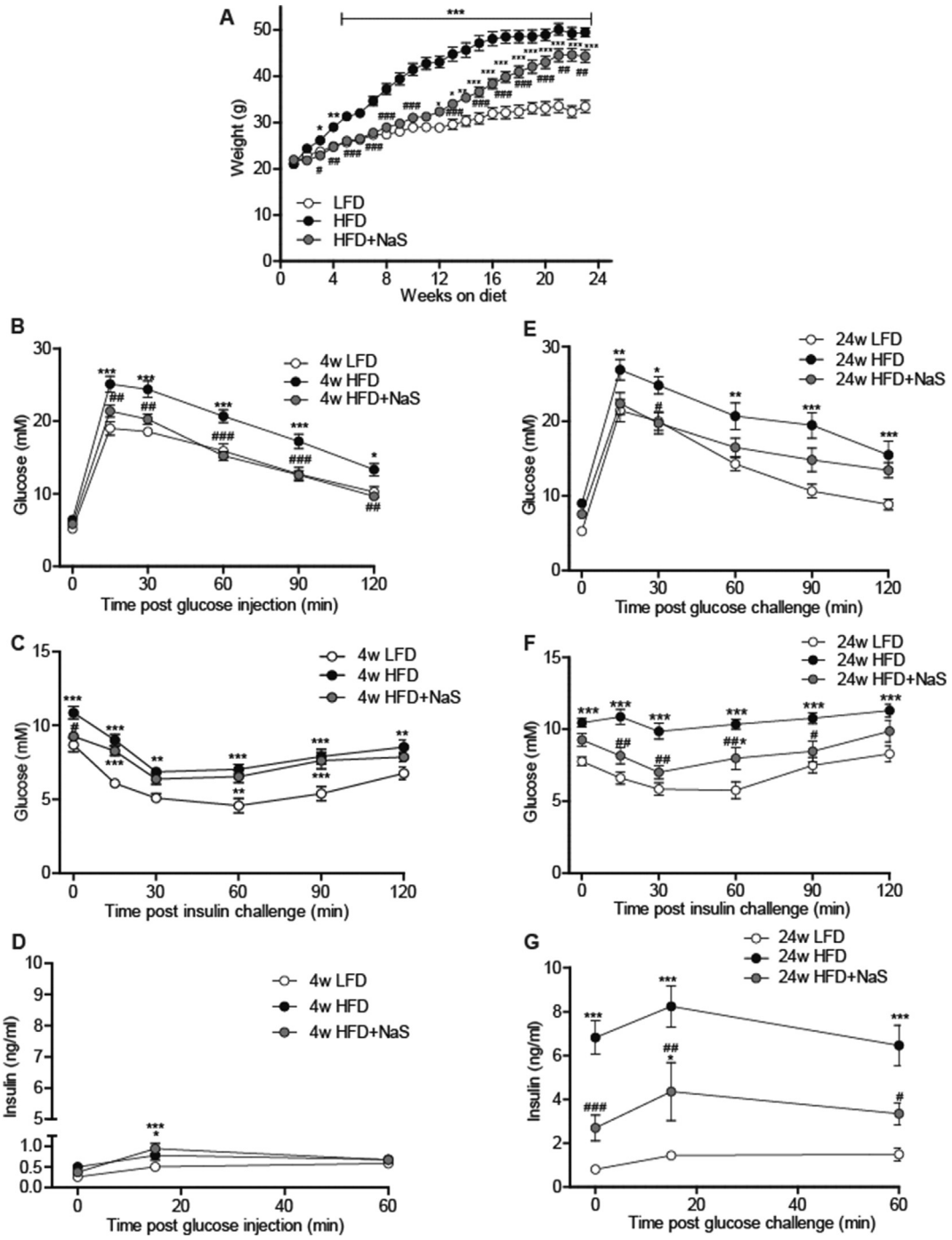

Figure 1: NaS delays weight gain and protects against HFD-induced insulin resistance. Male C57BL/6J mice were fed HFD (60% kcal from fat) with (grey circles) or without (black circles) NaS (6 g/kg diet) or LFD (10% kcal from fat) (white circles) for 24. (A) Bodyweight was measured weekly over 24w. (B&E) Glucose tolerance tests (GTT) were performed in overnight fasted mice after (B) 4w or (E) 24w HFD ± NaS. Mice were injected intraperitoneally with glucose (1.5 g/kg glucose), and blood samples collected by tail vein bleeding were taken at indicated time-points post-injection. (C&F) Insulin sensitivity was determined in mice that were fasted for 6h by intraperitoneal injection with insulin (0.5 units/kg insulin) and blood glucose levels quantified at indicated timepoints after (C) 4w and (F) 24w HFD ± NaS. (D&G) Insulin levels were monitored by ELISA at indicated time-points during the GTT after (D) 4w and (G) 24w HFD ± NaS; n = 16 per group; *p < 0.05, **p < 0.01, ***p < 0.001, w.r.t LFD; #p < 0.05, ##p < 0.01, ###p < 0.001, HFD vs. HFD + NaS for all graphs.

proteomics software package. Perseus statistical software was used to analyze the LFQ intensities. Differentially expressed proteins were inputted for pathway analysis through Ingenuity Pathway Analysis (IPA) and Cytoscape software.

2.7. Laboratory methods

Detailed description of methodologies including glucose and insulin tolerance testing, lipoprotein analysis, acylcarnitine measurement, FPLC, real-time PCR, energy expenditure studies, stromal vascular

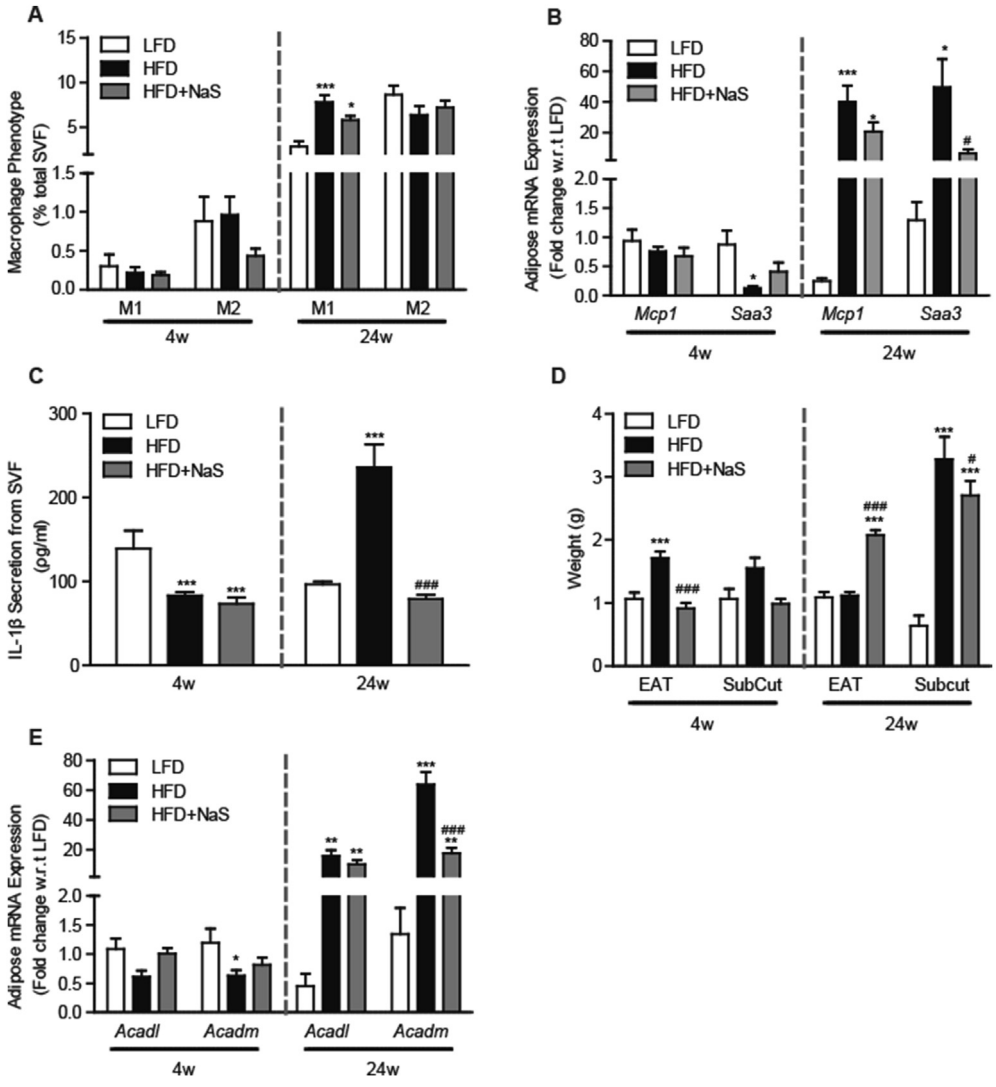

Figure 2: NaS attenuates adipose tissue inflammation. Male C57BL/6J mice were fed LFD, HFD or HFD + NaS (6 g/kg diet) for 4w or 24w. The stromal vascular fraction (SVF) cells were extracted from epididymal adipose tissues (EAT) via collagenase digestion. (A) Flow cytometry analyses of M1 (F4/80+, CD11C+, and CD206 (dim)) and M2 (F4/80+, CD11C- and CD206 (bright)) macrophages in SVF of adipose tissue (n = 6–8). (B) Gene expression analysis of Mcp1 and Saa3 in EAT as measured by real-time PCR (n = 8, normalized to LFD control). (C) SVF (1 × 106 cells/ml) were cultured overnight in complete media + LPS (100 ng/mL) for 24 h followed by ATP (5 mmol/L) stimulation for 1h. IL-1β levels in cell culture media was determined by ELISA (n = 4–5). (D) Weight of EAT and subcutaneous (SC) adipose tissue depots after 4w or 24w on LFD or HFD ± NaS (n = 8–17). (E) Gene expression analysis of Acadl and Acadm in adipose tissue from mice fed LFD or HFD ± NaS after 4 and 24w, as measured by real-time PCR (n = 8, normalized to LFD control). *p < 0.05, **p < 0.01, ***p < 0.001 w.r.t. LFD; #p < 0.05, ##p < 0.01, ###p < 0.001, HFD vs. HFD + NaS for all graphs.

fraction (SVF) isolation, and immunoblot analysis are available in the Supplemental Section.

2.8. Statistical analysis

Our primary outcome included changes in RCT in response to NaS intervention relative to HFD alone; our secondary endpoints were changes in adipose IL-1β secretion and changes in hepatic protein expression in response to HFD ± NaS. Sample size calculations were based on previous variance (~15%) between lean and obese mice in plasma ^{3}H-cholesterol levels at 4h during RCT studies; $\mu1 = 0.458$; $\mu2 = 0.389$ and pooled variance $\sigma = 0.07$, where $N = 2\sigma^2 (z_{\alpha/2} + z_{\beta})^2/(\mu1 - \mu2)^2$. Data are reported as mean ± SEM; each animal was considered an experimental unit. For comparison across multiple groups, data were tested for normal Gaussian distribution by the Shapiro–Wilk test. Normally distributed raw or log-transformed data ($n \geq 8$), were tested by one-way or two-way analysis of variance (ANOVA) as appropriate and when significant Bonferroni post-hoc tests were applied. Data-sets with $n < 8$ or non-normally distributed data underwent Kruskal–Wallis testing with Dunn's post-hoc test. GraphPad Prism version 5 (GraphPad Software Inc., CA) was used for statistical analyses. Statistical significance is presented as means (SEM) *p < 0.05, **p < 0.01 and ***p < 0.001 w.r.t. LFD or #p < 0.05, ##p < 0.01, ###p < 0.001 HFD v HFD + NaS for all graphs. For the acylcarnitines, the p-values were corrected for multiple testing using a False Discovery Rate (FDR) approach.

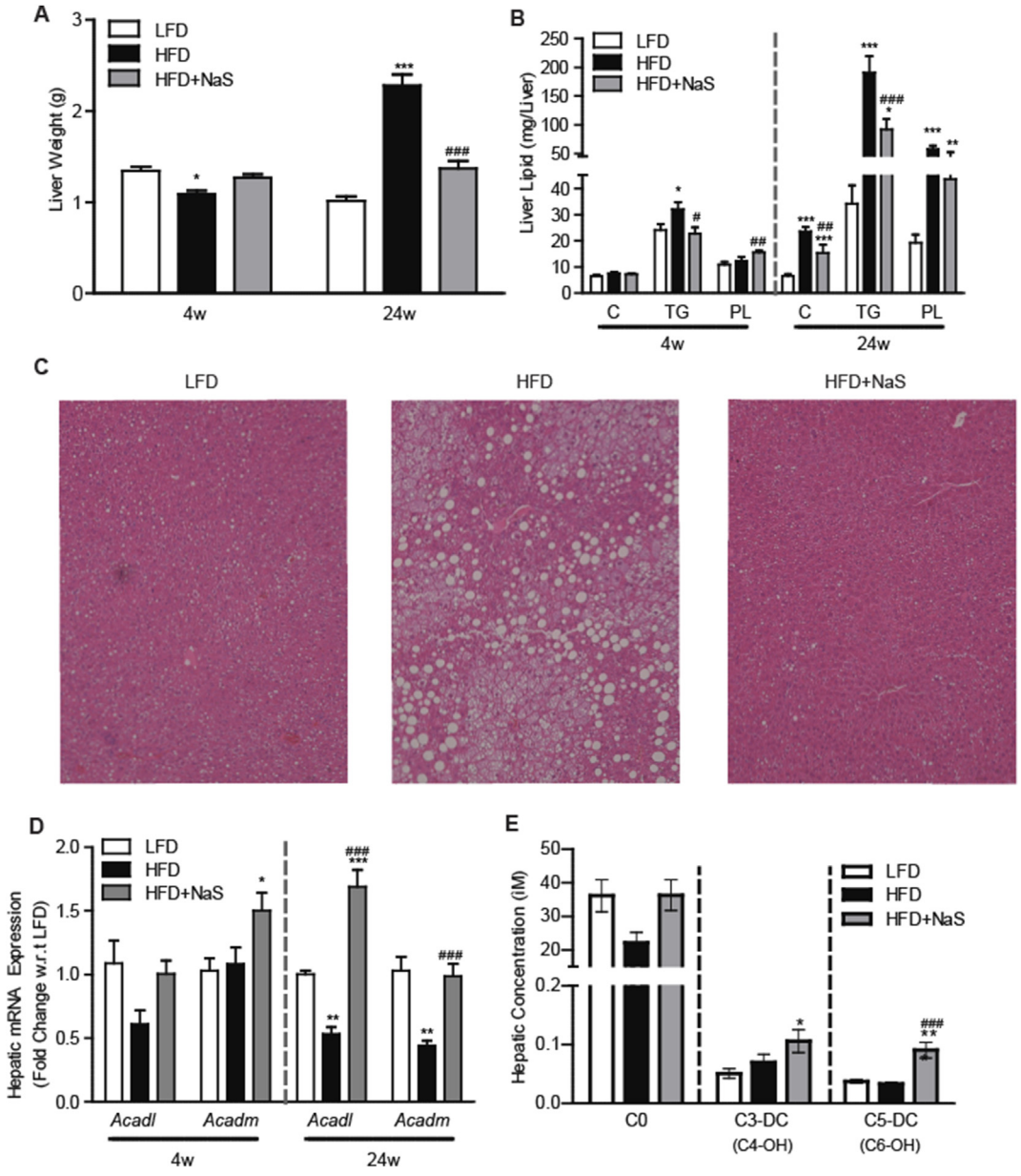

Figure 3: NaS protects against HFD-induced hepatosteatosis. Male C57BL/6J mice were fed LFD, HFD or HFD + NaS (6 g/kg diet) for 4w or 24w and the development of hepatosteatosis was subsequently investigated. (A) Liver weight at 4w (n = 8) and 24w (n = 16). (B) Hepatic lipid was monitored by enzymatic quantitation of cholesterol (C), triglycerides (TG), and phospholipids (PL) at 4 and 24w (n = 8–16). (C) Hematoxylin and eosin staining of paraffin-embedded hepatic samples confirmed lipid profile at 24w (n = 4). (D) Hepatic mRNA expression of Acadl and Acadm from mice fed LFD or HFD ± NaS after 4 and 24w, as measured by real-time PCR (n = 8, normalized to LFD control). (E) Acylcarnitine levels were determined in livers after 24w (n = 8). *p < 0.05, **p < 0.01, ***p < 0.001, w.r.t. LFD; #p < 0.05, ##p < 0.01, ###p < 0.001, HFD vs. HFD + NaS for all graphs.

3. RESULTS

3.1. NaS delays weight gain and protects against HFD-induced insulin resistance

Supplementation of an HFD with NaS (NaS + HFD) protected against weight gain during weeks 1–12 despite increased caloric consumption compared to supplementation of both LFD and HFD (Figure 1A and Supplemental Fig. 1A). Rapid weight gain was subsequently observed from 12 to 20 w before plateauing at levels that remained significantly lower than HFD alone (Figure 1A). Energy expenditure analysis was performed after 4w HFD ± NaS but no significant changes were observed (Supplemental Figs. 1B–D). Furthermore, contrary to previous findings [27], we found a significant reduction in uncoupling protein 1 (UCP-1) mRNA within brown adipose tissue with HFD + NaS relative to LFD (Supplement Figure 1E).

NaS protected against HFD-induced glucose intolerance, insulin resistance, and hyperinsulinemia after 4w-HFD (Figure 1B–D), and 24w-HFD (Figure 1E–G), with GTT profiles akin to LFD counterparts, despite the obese phenotype at 24w (Supplemental Fig. 1F). There was progressive deterioration in Homeostatic Model Assessment for Insulin

Table 1 — Body weight, plasma parameters, liver weight and liver lipid profile in C57BL/6Jmice fed LFD ($n = 14$), HFD ($n = 16$) or HFD + NaS (n = 16) for 24w. *p < 0.05, **p < 0.01, ***p < 0.001 w.r.t. LFD; $^{\#}p < 0.05$, $^{\#\#}p < 0.01$ and $^{\#\#\#}p < 0.001$ HFD vs. HFD + NaS.

Clinical parameters	LFD	HFD	HFD + NaS
Body Weight (g)	33.4 ± 1.3	48.9 ± 0.9***	44.3 ± 1.4***
Plasma Glucose (mM)	5.3 ± 0.3	9.0 ± 0.6	7.6 ± 0.4
Plasma Insulin (ng-mL-1)	0.8 ± 0.1	6.8 ± 0.8***	2.7 ± 0.6###
HOMA-IR	5.5 ± 0.9	82.7 ± 11.7***	25.1 ± 5.0###
Plasma total Cholesterol (mg/dL)	127.5 ± 7.7	228.4 ± 13.5***	200.4 ± 15.2**
Plasma HDL-Cholesterol (mg/dL)	100.6 ± 6.4	130.94 ± 11.4	103.8 ± 8.1
Plasma non-HDL-C (mg/dL)	33.4 ± 8.9	97.42 ± 18.5*	102.7 ± 16.5**
Plasma Triglycerides (mg/dL)	101.8 ± 11.2	130.5 ± 12.1*	99.2 ± 8.2
Plasma Phospholipids (mg/dL)	263.1 ± 19.2	353.7 ± 20.5*	294.4 ± 11.3
Plasma ALT (nmol/min/mL)	0.9 ± 0.5	11.5 ± 3.0***	2.4 ± 1.0##
Plasma AST (nmol/min/mL)	10.0 ± 2.4	13.1 ± 2.3	3.5 ± 1.6#
Liver Weight (g)	1.0 ± 0.04	2.3 ± 0.1***	1.4 ± 0.1**###
Hepatic Cholesterol (mg/liver)	6.6 ± 0.6	23.6 ± 1.7***	15.3 ± 3.2***##
Hepatic Triglycerides (mg/liver)	34.2 ± 7.0	190.9 ± 28.1***	91.8 ± 18.1*###
Hepatic Phospholipids (mg/liver)	19.2 ± 3.1	57.5 ± 6.2***	43.6 ± 8.6**

Resistance (HOMA-IR) scores between 4 and 24w HFD (Supplemental Fig. 1G). HOMA-IR was significantly attenuated by NaS at 24 w relative to HFD alone (Supplemental Fig. 1G).

3.2. NaS suppresses IL-1β secretion from an adipose-derived stromal vascular fraction (SVF) after 24w HFD

Increased recruitment of pro-inflammatory M1 macrophages into EAT, was observed after 24w on both HFD and, to a lesser extent on HFD + NaS, relative to on LFD (Figure 2A), mirroring trends in monocyte chemoattractant protein (MCP)-1 mRNA expression (Figure 2B). Serum amyloid A3 (SAA3), another key marker of adipose tissue inflammation, was increased after 24w HFD relative to LFD and was significantly reduced after HFD + NaS relative to HFD alone (Figure 2B). IL-1β secretion from an adipose-derived SVF stimulated *ex vivo* with LPS + ATP, was significantly increased after 24w on HFD relative to LFD (Figure 2C). NaS abrogated this elevation in IL-β secretion from HFD-derived SVF (Figure 2C). Similar results were found for TNF-α secretion from SVF at 24w (Supplemental Fig. 1H). At the 4w time-point, there was no evidence of inflammatory macrophage cell infiltration into adipose tissue (as reported previously [13]), no evidence of IL-1β priming, and no significant difference observed in MCP-1 and SAA3 across groups. This indicated that this early phase of insulin resistance is not related to adipose inflammation (Figure 2A—C).

EAT weight was significantly increased after 4w HFD, but not 24w HFD, relative to LFD (Figure 2D). Interestingly, the EAT depot expanded in mice fed HFD + NaS at 24w relative to mice fed both LFD and HFD, indicative of greater functionality of this depot, and was coincident with reduced hepatosteatosis. By contrast, the subcutaneous adipose depot significantly expanded after HFD, and to a lesser extent HFD + NaS, relative to LFD at 24w (Figure 2D). Furthermore, the EAT morphology was improved after 24w HFD + NaS relative to HFD alone, with a more uniform adipocyte size evident with NaS treatment (Supplement Figure 1I&J). NaS did not significantly alter the expression of acyl Co-A dehydrogenase long-chain *(Acadl)* and acyl-CoA dehydrogenase medium-chain *(Acadm)* in EAT at 4w relative to HFD. After 24w of feeding HFD, expression of *Acadm* in EAT was significantly reduced after HFD + NaS relative to HFD indicating that enhanced oxidation through white adipose tissue does not underlie reduced weight-gain (Figure 2E). A potent increase in expression of *Acadl* and *Acadm* was evident in EAT after 24w HFD (with and without NaS) relative to LFD, indicative of a metabolic fuel switch within adipose tissue to predominantly fatty acid oxidation (Figure 2E).

3.3. NaS protects against HFD-induced hepatosteatosis

NaS supplementation resulted in profound protection against hepatic lipid accumulation with liver-weights equivalent to LFD after both 4w and 24w HFD (Figure 3A). Hepatic accumulation of triglycerides, cholesterol, and phospholipids was attenuated after feeding HFD + NaS compared to HFD alone at 24w (Figure 3B) which was confirmed by histological hematoxylin and eosin (H&E) staining (Figure 3C). mRNA expression of the β-oxidation genes, *Acadm* and *Acadl,* was suppressed after 24w on HFD relative to on LFD (Figure 3D). By contrast, mRNA expression of *Acadm* was preserved and expression of *Acadl* was increased after HFD + NaS compared to LFD, indicating that enhanced β-oxidation within this group may protect against steatosis (Figure 3D). Analysis of acyl-carnitine levels in the liver demonstrated a significant increase in short/medium-chain acylcarnitines (C3 and C5 length) with NaS relative to both LFD and HFD, again indicative of enhanced fatty acid oxidation in response to NaS (Figure 3E and Supplemental Table 1). This significance was retained for C5-length acylcarnitines only upon correction for FDR (p-value 9.8004E-4). A significant increase in alanine transaminase (ALT) levels was also evident after 24w HFD relative to LFD, an effect that was blunted by the NaS supplementation (Table 1). Minimal perturbations in hepatic lipids were evident after 4w HFD relative to LFD (Figure 3A,B & D and Supplement Table 2).

3.4. NaS reconfigures metabolic pathways in the liver with increased activation of PPAR-alpha pathways and decreased activation of LXR/RXR pathway

To further probe the underlying mechanisms contributing to reduced steatosis with NaS relative to HFD alone, we analyzed the liver proteome. Chronic HFD resulted in differential expression of 600 hepatic proteins relative to LFD including reduction in proteins involved in glycolysis, the TCA cycle and the electron transport chain and increased expression of proteins involved in fatty acid oxidation, and proteins regulated by both PPAR and LXR transcription factors (Supplement Figure 2 and Supplement Table 3). NaS intervention significantly altered 484 liver proteins relative to HFD (Supplement Table 4). Primary pathways activated by NaS included fatty acid beta-oxidation, tryptophan metabolism, amino acid metabolism, the TCA cycle, and the electron transport chain, while glycolytic, LXR/RXR, and IL-1 mediated inhibition of the retinoid X receptor (RXR) pathways were reduced relative to HFD (Figure 4A—C). PPARα-proteins in particular were upregulated by NaS relative to HFD (Figure 5 and Supplement Table 4). Proteins involved in fatty acid oxidation including acyl-CoA synthetase Long-Chain Family Member 1 (ACLS1), *Acadm, Acadl*, enoyl-CoA delta isomerase 1 and 2 (ECI1 and ECI2) and acetyl coA Acyltransferase 2 (Acca2) were upregulated after HFD + NaS relative to HFD. Levels of malonyl CoA decarboxylase (MCD), a negative regulator of *de novo* lipogenesis, were also upregulated with the HFD + NaS diet relative to HFD (Supplemental Figs. 3A—B). A corresponding reduction in expression of glycolytic proteins was evident with HFD + NaS relative to HFD including glucose-6-phosphate isomerase (GPI) and pyruvate kinase L/R (PKLR) (Supplemental Figs. 3C—D).

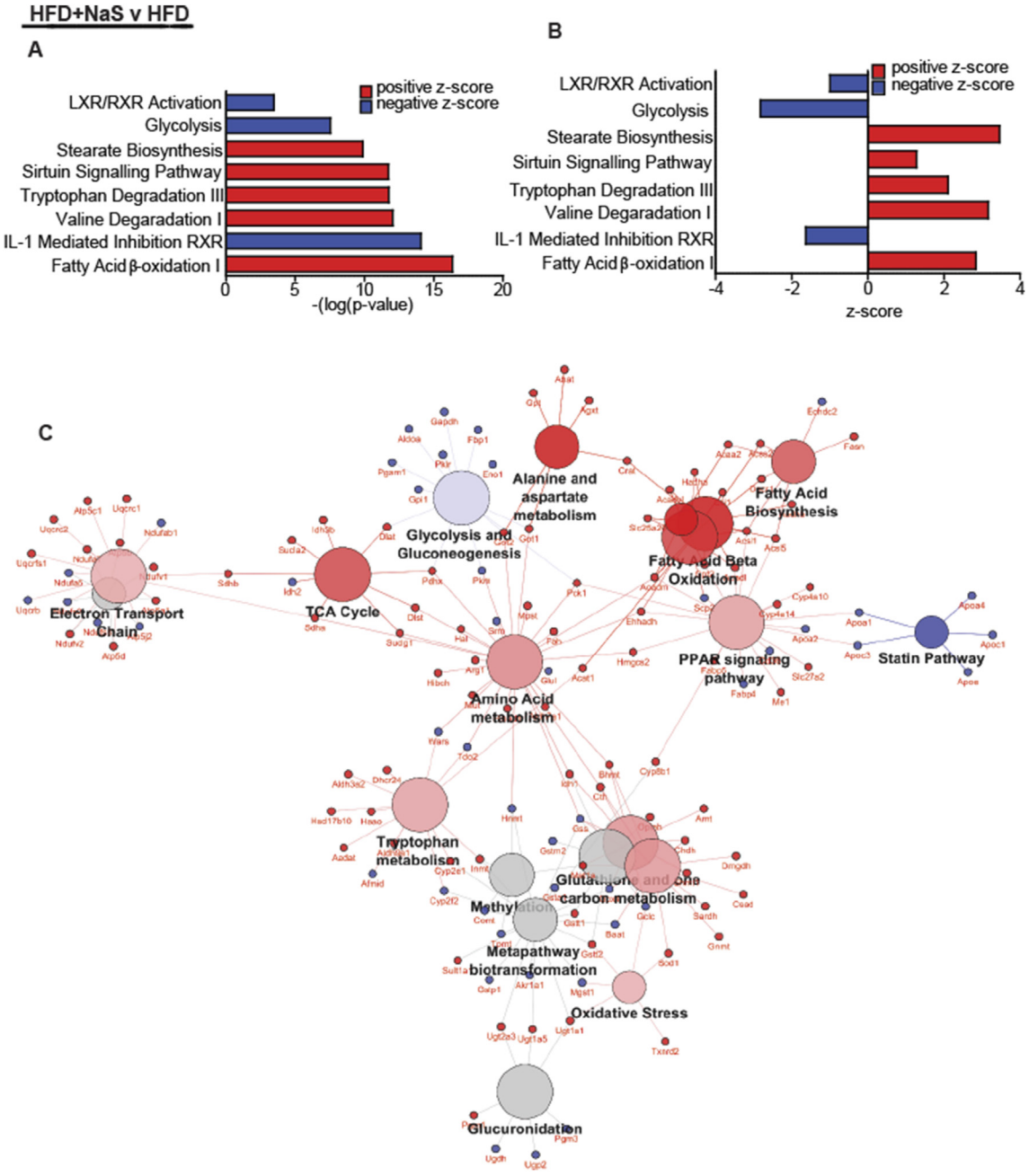

Figure 4: Hepatic proteomic analysis identifies key metabolic pathways modulated by NaS. Male C57BL/6J mice were fed LFD, HFD or HFD + NaS (6 g/kg) for 24w. Liver tissue was harvested and proteins isolated using RIPA buffer. Protein was precipitated using trichloroacetic acid (20%), and in-solution digestion performed overnight. Peptide fractions were analyzed on a quadrupole Orbitrap (Q-Exactive, Thermo Scientific) mass spectrometer equipped with a reversed-phase NanoLC UltiMate 3000 HPLC system (Thermo Scientific). Label-free quantitative (LFQ) ion intensities were generated by using the default setting of MaxQuant. Proteins that were significantly different between HFD and HFD + NaS groups were determined by using Perseus statistical software ($n = 7-8$, #$P < 0.05$ w.r.t. HFD). IPA pathway analysis revealed key regulatory pathways that are most differentially modulated with (A) −(log)p-value and (B) z-score presented. (C) Networks were visualized as pathways that are upregulated (red) and downregulated (blue) as illustrated by Cytoscape software.

Hepatic expression of apolipoproteins (Apo), regulated by LXR, including ApoA1, ApoA2, ApoA4, ApoC3, and ApoE were upregulated after HFD relative to both LFD and HFD + NaS (Figure 6D). The S100-family of proteins, including S100A8, S100A9, and S100A10 was also significantly increased after HFD, but not HFD + NaS, relative to LFD (Supplement Figure 4A&B). NaS increased the expression of the RXR-target protein mitochondrial 3-hydroxy-3-methylglutaryl CoA synthase 2 (HMGCS2), a key protein in ketogenesis [29] but failed to recover HFD-induced repression of ABCB11 relative to LFD (Supplemental Figs. 4C–D).

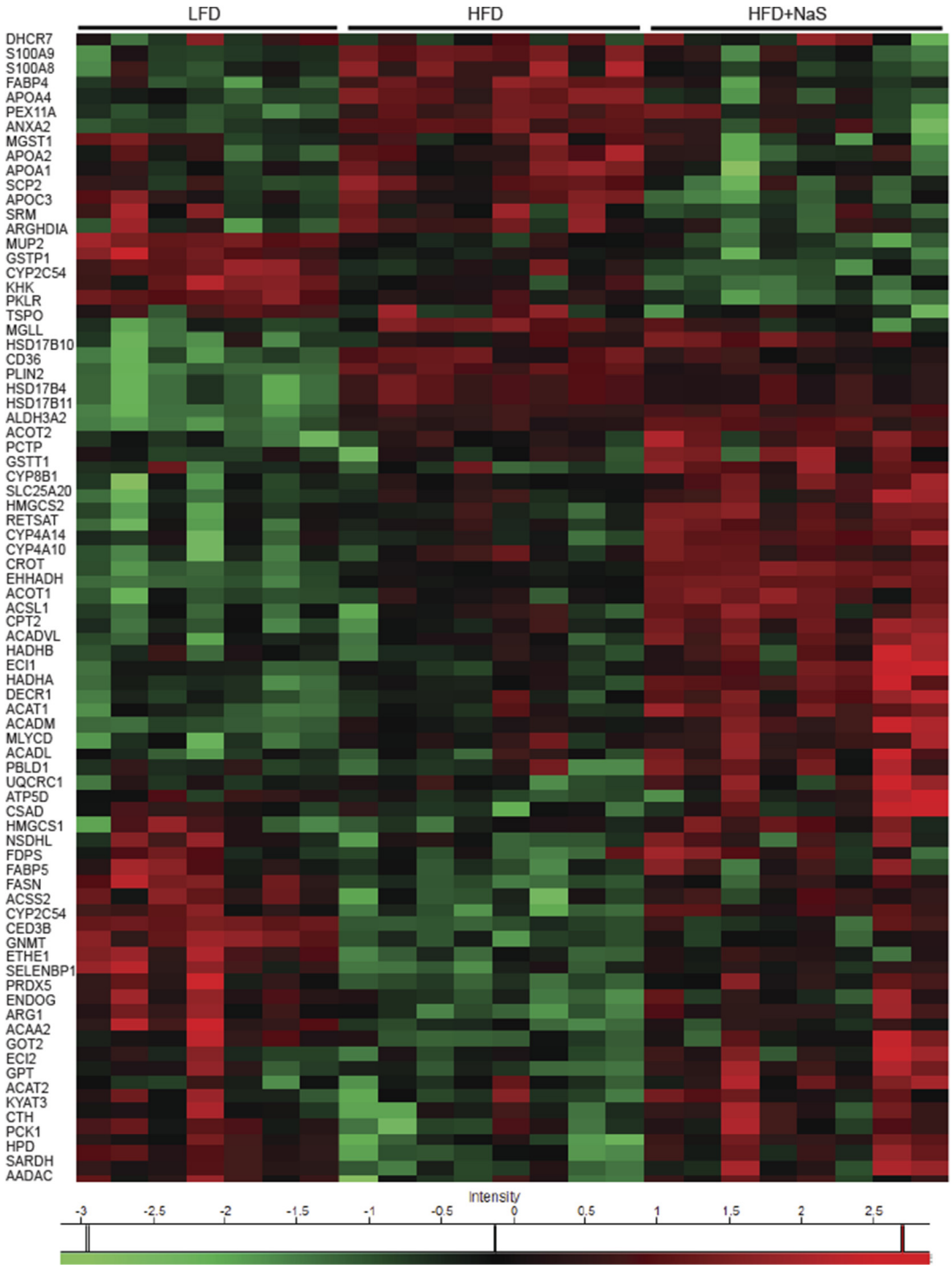

Figure 5: NaS intervention modulates expression of PPARα-regulated proteins. Male C57BL/6J mice were fed LFD, HFD or HFD + NaS (6 g/kg) for 24w. Liver proteins were harvested in RIPA buffer, precipitated with 20% TCA and in-solution digestion was performed overnight. Label-free quantitative (LFQ) ion intensities were generated using the default setting of MaxQuant. Proteins that were significantly different between HFD and HFD + NaS groups were determined using Perseus statistical software ($n = 7-8$, #$p < 0.05$ w.r.t. HFD). IPA pathway analysis revealed modulation of upstream regulator pathway 'PPARα'. (A) Heat map generated using Perseus including PPAR-alpha proteins differentially modulated by HFD + NaS relative to HFD; red color indicating upregulation and green color indicating down-regulation.

3.5. The HDL proteome switches toward an anti-thrombotic phenotype and mirrors numerous changes observed in the hepatic proteome

Supplementation of HFD with NaS resulted in the reduced association of coagulation factor IX and pro-thrombin and increased association of anti-thrombin within HDL-fractions relative to HFD (Figure 6A—B). Interestingly, patterns in hepatic protein expression of apolipoproteins were reflected within the HDL proteome with an increased association of ApoA1, ApoA2, ApoA4, ApoC3, and ApoE evident on HFD-HDL relative to LFD-HDL (Figure 6C); these effects were attenuated with

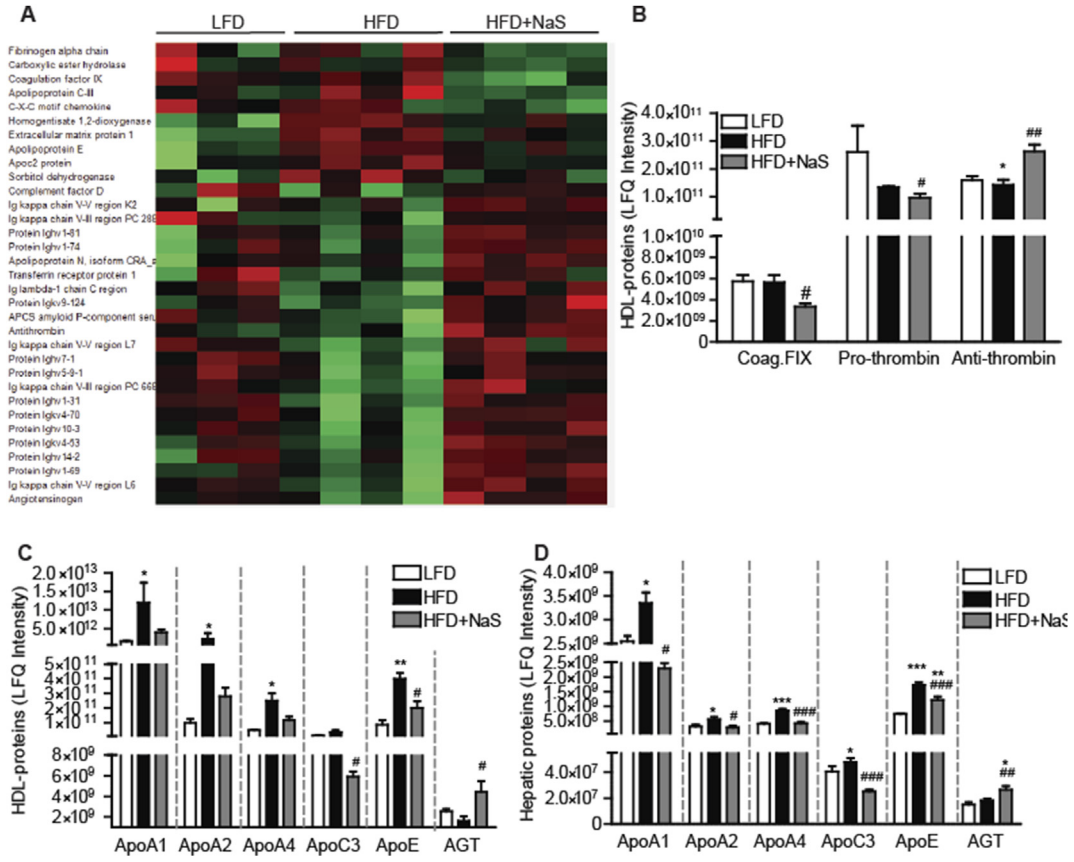

Figure 6: Trends in HDL-associated apolipoproteins mirror patterns in liver protein expression. Male C57BL/6J mice were fed LFD, HFD or HFD + NaS (6 g/kg) for 24w. Plasma was harvested and separated by FPLC and protein content in HDL-containing fractions 36–38 was precipitated using 20% TCA, and in-solution digested overnight, prior to proteomics analysis. Label free quantitative (LFQ) ion intensities were generated by using the default setting of MaxQuant. (A) Proteins that were significantly different on HDL between HFD and HFD + NaS groups were determined using Perseus statistical software and a heat-map was generated ($n = 3$–4, $^{\#}P < 0.05$ w.r.t. HFD). (B) Levels coagulation factor IX, prothrombin, anti-thrombin on HDL are presented across all groups. (C&D) Levels of apolipoproteins (ApoA1, A2, A4, C3, E) and angiotensinogen within (C) HDL-fractions and (D) liver are presented across all groups. *p < 0.05, **p < 0.01 and ***p < 0.001 w.r.t LFD; $^{\#}P < 0.05$, $^{\#\#}P < 0.01$ and $^{\#\#\#}P < 0.001$ HFD vs. HFD + NaS.

NaS in both the liver and HDL-proteome (Figure 6C–D). Of interest, and warranting caution, NaS significantly increased hepatic protein levels of angiotensinogen (AGT), a protein involved in blood pressure regulation, which translated to increased HDL-associated AGT in circulation (Figure 6C–D).

3.6. NaS preserves HDL-CEC but has minimal impact on HFD-induced hypercholesterolemia

Despite the remarkable improvements seen in hepatosteatosis after 24w HFD + NaS relative to HFD alone, only a marginal reduction in total cholesterol levels was observed (Table 1 and Figure 7A). Greater reductions in systemic triglyceride and phospholipid levels were observed with HFD + NaS compared to 24w-HFD (Table 1). Reduced HDL-CEC, particularly ABCA1-independent CEC, was evident after 24w HFD, but not after HFD + NaS, relative to LFD, indicative of a protective effect of NaS on particle functionality (Figure 7B). Increases in HDL-C after HFD partially compensated for the development of HDL dysfunction (Supplemental Fig. 5A). As demonstrated previously [9] there was a significant increase of ^{3}H-cholesterol in plasma and liver after 24w HFD relative to LFD during RCT (Figure 7C–D) that did not translate to increased ^{3}H-cholesterol fecal elimination (Figure 7E). No difference in the distribution of ^{3}H-tracer across bile-acids or sterol compartments in feces, or ^{3}H-tracer in bile, was evident across groups (data not shown). Accumulation of ^{3}H-cholesterol within plasma and liver compartments was attenuated with NaS (Figure 7C–D) indicative of a partial improvement in cholesterol trafficking. Nonetheless, no significant rescue in HFD-induced repression of ABCG5/8 and ABCB11 mRNA or protein expression was observed with NaS (Figure 7F and Supplement Figure 7). HDL function and macrophage-to-feces RCT were unaffected after 4w HFD (Supplemental Figs. 6A–E), indicating that obesity-impaired RCT occurs secondary to metabolic perturbations of obesity and not as a direct result of exposure to an HFD alone.

4. DISCUSSION

In this study, we demonstrate for the first time that long-term NaS supplementation within an obesogenic diet potently suppressed IL-1β secretion from adipose SVF and rewired hepatic metabolic pathways to enhance fatty acid beta-oxidation and reduce LXR/RXR pathway activation. Mice consuming HFD + NaS exhibited significantly reduced insulin resistance, hyperinsulinemia, and hepatosteatosis relative to those consuming HFD alone, despite the development of the obese phenotype at 24w. NaS also preserved HDL-CEC and prevented HFD-induced ^{3}H-cholesterol accumulation within the plasma and liver compartments during RCT. Notwithstanding, NaS showed minimal effect on HFD-induced hypercholesterolemia and failed to rescue hepatic ABCG5/

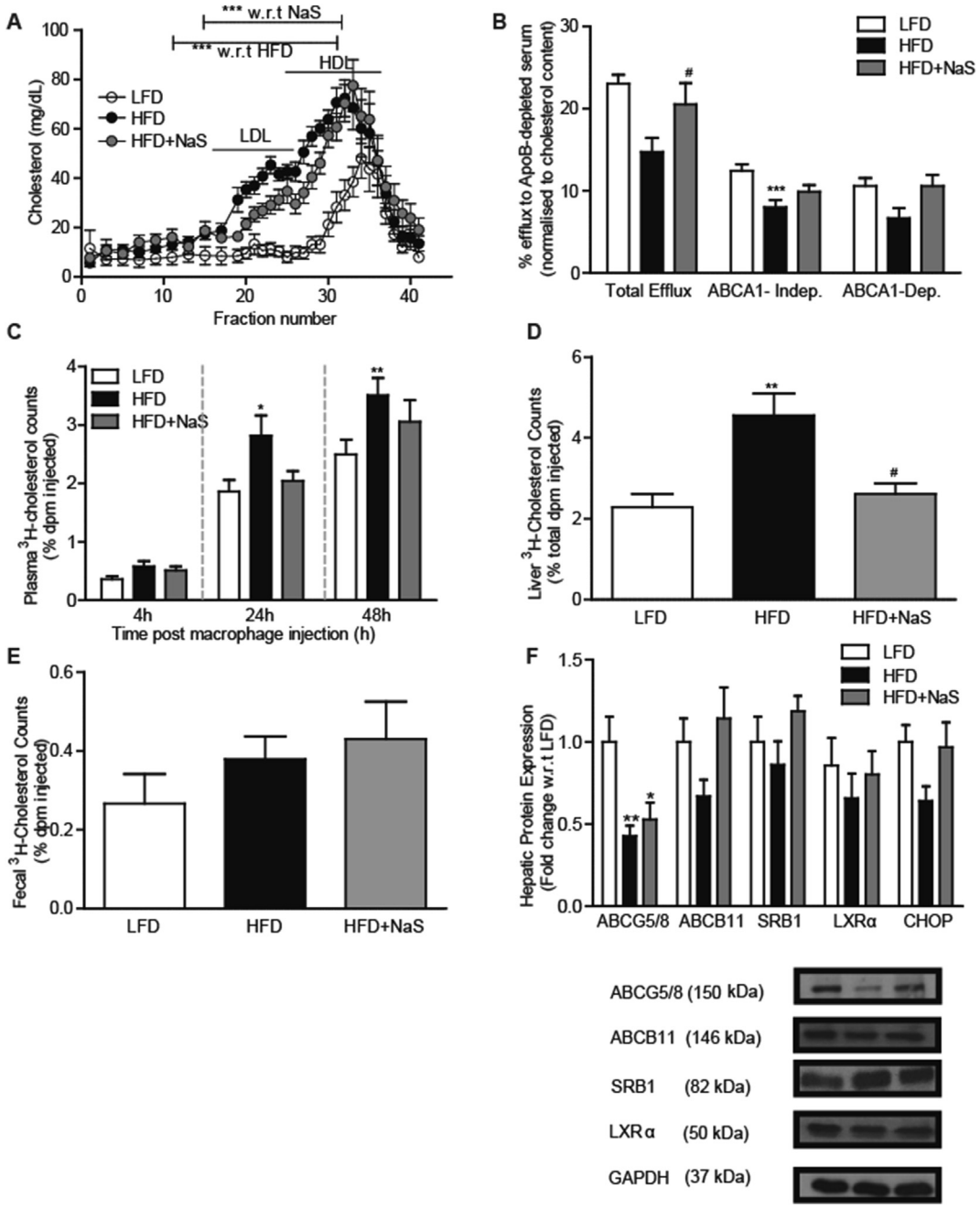

Figure 7: NaS supplementation partially attenuates HFD-induced hyperlipidemia and prevents plasma and hepatic ^{3}H-cholesterol accumulation during RCT. Male C57BL/6J mice were fed LFD, HFD or HFD + NaS (6 g/kg diet) for 24w. (A) Plasma lipoproteins were separated by FPLC and cholesterol levels in fractions determined enzymatically (n = 16). (B) ApoB particles were removed from the plasma by PEG precipitation resulting in an HDL-enriched supernatant. J774 macrophages, pre-labeled with 3H-cholesterol (1 μCi/mL) for 24h, were stimulated ± cAMP (0.3 mmol/L) to drive ABCA1 protein expression. The percentage of 3H-cholesterol efflux to 2.8% PEG supernatant was monitored over 4h and normalized to HDL-C concentrations. Total efflux was determined from cells stimulated + cAMP; ABCA1-independent efflux was measured from unstimulated cells (-cAMP); ABCA1-dependent efflux was calculated as the difference in efflux from cells stimulated in the presence and absence of cAMP. (C–F) C57BL/6J mice were injected intraperitoneally with 3H-cholesterol–labeled macrophages (~2 × 106 cells/4 × 106 dpm/mouse) after 24 weeks on LFD, HFD, and HFD + NaS. (C) Plasma 3H-cholesterol levels were monitored over 48h by liquid scintillation counting (LSC). After 48h, mice were euthanized, and (D) hepatic and (E) fecal 3H-cholesterol counts were measured by LSC. (F) Hepatic protein expression of proteins involved in cholesterol homeostasis was determined by immunoblot analysis. Protein bands were quantified by densitometry and normalized to Glyceraldehyde 3-phosphate dehydrogenase (GAPDH) levels. A representative immunoblot is shown (n = 6–8). Additional blots are presented in Supplemental Fig. 7. *p < 0.05, **p < 0.01, ***p < 0.001, w.r.t. LFD; #p < 0.05, ##p < 0.01, ###p < 0.001, HFD vs. HFD + NaS for all graphs.

8 or ABCB11 expression. These findings suggest that the development of steatosis is not a pre-requisite for perturbations in cholesterol homeostasis in obesity, and enhanced oxidation of fatty acids similarly does not infer improvements in cholesterol homeostasis and indeed may provide ample substrate for cholesterologenesis.

Chronic exposure to SFA-HFD primes pro-IL-1β within adipose immune cell populations resulting in enhanced IL-1β secretion *ex vivo* upon exposure to a second hit (LPS/ATP) [15]. Enhanced responsiveness of HFD-derived adipose SVF to LPS/ATP was abrogated with NaS supplementation in the current study. This suggested reduced priming of pro-IL1β within SVF-resident immune cells. A significant increase in both pro-inflammatory M1 macrophage number and MCP1 expression was observed following HFD ± NaS at 24w relative to LFD, indicative that reduced immune cell number does not underpin reduced IL-1β secretion with NaS. Notably, there was no evidence of adipose tissue inflammation after 4w HFD, thus confirming the progressive nature of obesity-associated metabolic perturbations. IL-1β has been implicated in the development of insulin resistance in murine models [14,17], potently impairing adipogenesis [30]. In this study, we demonstrate that the EAT depot initially expands after 4w HFD but undergoes retraction by 24w HFD with preferential deposition of fat within the subcutaneous depot. The EAT depot was significantly heavier after 24w on HFD + NaS relative to HFD alone, despite lower overall body weight, with significant improvement in adipose morphology evident. Duval et al. previously demonstrated that HFD-fed mice with high levels of steatosis (HFD + steatosis) exhibited lower EAT weight despite the greater overall weight gain, and increased expression of inflammatory markers, and increased immune cells within EAT, compared to HFD-fed mice with low levels of steatosis [31]. Our findings corroborate these previous findings although the underlying mechanisms remain poorly defined. Furthermore, we could not confirm whether the suppressive effects of NaS on IL-1β in adipose tissue positively impact the liver or if enhanced utilization of fatty acids by the liver is central to inhibition of IL-1β priming within adipose tissue.

To date, the impact of salicylates has shown encouraging results within glycaemic management [32,33]. Murine studies have shown metabolic improvements with NaS consistent with reduced weight gain and reduced hepatosteatosis in short-term feeding studies (<12w) in previous studies [27,34,35]. Liang et al. in a 12w study, demonstrated a correlation of reduced weight-gain/steatosis with NaS with the induction of hepatic lipid-metabolism genes by microarray analysis [34]. Smith et al. reported that salsalate therapy (8w) improved glucose tolerance and reduced lipid liver content in an AMPK-independent manner [35]. Furthermore, salsalate increased oligomycin-insensitive respiration causing mitochondrial uncoupling which was associated with reduced lipogenesis [35]. Van Dam et al. identified enhanced activation of brown adipose tissue within mice fed on salsalate for 12w coincident with protection against weight gain [27]. Salsalate therapy also induced weight loss in mice pre-fed an HFD for 12w with a significant reduction in hepatosteatosis [27]. Our data have demonstrated for the first time that the beneficial effects of salicylate on weight gain are temporary with a catch-up phase evident between 12-24w HFD. Contrary to findings in Van Dam et al. [27], we observed neither an increase in UCP-1 mRNA levels within BAT nor overt differences in energy expenditure at the 4w time-point; however, it is notable that we only assessed mRNA levels and cannot infer lack of induction of UCP-1 protein and/or UCP-1 activity in our studies. Our data suggest an important role for enhanced hepatic beta-oxidation in driving cardiometabolic health benefits with NaS.

In short-term feeding studies, it has been difficult to extrapolate whether the reduction in hepatosteatosis is a consequence of reduced weight gain or whether enhanced hepatic β-oxidation prevents weight gain. Our study demonstrates that even after significant weight gain with NaS at 24w, there remains significant protection against hepatosteatosis coincident with increased activation of proteins involved in hepatic β oxidation. Reduced steatosis can be driven via reduced lipogenesis or via enhanced oxidation of fatty acids. Insulin, a critical hormone, stimulates hepatic glycolysis to generate acetyl CoA, the key substrate for lipogenesis [36]. NaS significantly reduced both fasting and postprandial insulin levels in obese mice relative to HFD alone and hepatic expression of the glycolytic proteins glucose-6-phosphate isomerase; pyruvate kinase L/R were also reduced after HFD + NaS relative to HFD, which may contribute to reduced lipogenesis. NaS also activates AMPK [26], which deactivates acetyl CoA carboxylase (ACC), a key enzyme in *de novo* fatty acid synthesis. In parallel, NaS activates MCD which promotes catabolism of the potent inhibitor of β-oxidation, malonyl CoA to preferentially stimulate fatty acid oxidation [37]. We similarly observed upregulation of MCD with NaS, likely contributing to enhanced β-oxidation with NaS. Increased expression of proteins involved in β-oxidation including Acadm, Acadl (first step of β oxidation), Acca2 (final step of β oxidation), ECI1 and ECI2 (β oxidation of unsaturated fatty acids), and ACLS1 (preparatory step for β-oxidation) was also evident with NaS relative to HFD alone. Proteins involved in the tricarboxylic acid (TCA) cycle) and electron transport chain were similarly upregulated with NaS intake indicative of enhanced oxidative phosphorylation (oxphos). Collectively these data demonstrate that NaS continues to protect against steatosis within the obese setting, likely by both suppressing lipogenesis and stimulating hepatic β-oxidation and oxphos.

Despite remarkable protection against hepatosteatosis and reduction in system TAG levels, NaS had minimal effect on HFD-induced hypercholesterolemia. Hepatic proteomics analysis suggests that NaS shunts excess acetyl CoA produced via increased fatty acid oxidation into ketogenic and cholesterologenic pathways with increased levels of HMGCS1 and HMGCS2 evident with HFD + NaS relative to HFD. Reduction in systemic triacylglycerolS (**TAG**), coupled with the lack of reduction in systemic cholesterol levels, could also be attributable to impaired clearance of very-low-density lipoprotein (VLDL) remnants from circulation but mechanistic kinetic studies would be required to probe this idea further. Notably, human clinical trials demonstrated that salsalate has successfully lowered fasting triglyceride concentrations in non-diabetic patients with insulin resistance [38] and patients with overweight/obesity and established heart disease [33] but failed to lower systemic cholesterol levels. The targeting inflammation using salsalate in CVD (TINSAL-CVD) trial also found no effect of salsalate (3.5 g/d over 30 months) on the progression of atherosclerosis beyond statin therapy, although the trial size was limited ($n = 129$) [33]. Faghihimani et al.also found no change in LDL-C in patients with Type 2 Diabetes Mellitus (T2DM) receiving salsalate (3 g/d for 12 weeks, n = 60) [39]. It is plausible that excess Acetyl CoA derived from increased fatty acid oxidation with NaS, beyond the body's energy requirements, provides ample substrate for cholesterologenesis which when coupled with reductions in liver cholesterol transporter expression may provide an ideal microenvironment to sustain hypercholesterolemia.

We previously demonstrated that long-term exposure to HFD impaired multiple steps of RCT including HDL-CEC and hepatic cholesterol trafficking [9]. In the current study, we demonstrate that this is a progressive paradigm, with no evidence of impaired RCT after 4w HFD. By 24w, HDL-CEC (normalized to HDL-C) was reduced after HFD relative to LFD, an effect that was attenuated by NaS. The increase in HDL-C after HFD partially compensates for this loss of function but is not sufficient to account for the significant increase in ^{3}H-cholesterol

that accumulates in plasma during RCT studies after HFD relative to LFD, indicative of a backlog of ^{3}H-cholesterol in circulation. Within this study, we demonstrate that NaS has anti-inflammatory effects within the adipose tissue, reduces systemic ALT levels, and reduces hepatic protein expression of S100 proteins that are known to accumulate at sites of chronic inflammation [40,41] in comparison to feeding HFD alone. Notwithstanding, HFD-induced repression of ABCG5/8 and ABCB11 protein expression was not rescued with NaS. ABCG5/8 are considered LXR-target genes that are upregulated by LXR agonism [42]. Reduced levels of liver cholesterol observed with NaS may cause reduced oxysterol substrate availability for LXR agonism [43] contributing to lack of apparent rescue of ABCG5/8. Notably, while many LXR target proteins are upregulated following HFD relative to LFD (e.g., apolipoproteins), ABCG5/8 expression (mRNA and protein) is counterintuitively reduced [9]. It is the LXR-binding partner retinoid-X-Receptor alpha (RXRα) that has binding sites within ABCG5/8 and ABCB11 genes, with little evidence for direct binding sites for LXR [44]. RXRα dimerizes with numerous transcription factors including PPARα and FXR [45], with FXR/RXR dimers governing ABCB11 expression [46,47]. Hence, it is plausible that disturbances in nuclear factor dimer formation and activation of metabolic pathways within the liver, independent of inflammation, may underpin differential regulation of LXR-induced proteins after HFD which remains to be investigated in the future.

We finally evaluated whether changes within hepatic metabolic pathways evident with HFD $\pm$ NaS would be reflected within the HDL proteome. There was a shift towards a more anti-thrombotic particle with NaS treatment, with an increased association of anti-thrombin and reduced association of pro-thrombin and coagulation factor IX, on circulating HDL relative to HFD-HDL. Furthermore, changes in the pattern of proteins on HDL reflected changes within the hepatic proteome, particularly the apolipoproteins, highlighting the promising potential of the HDL proteome to detect changes within hepatic metabolic pathways, within an easily accessible biofluid.

Limitations of the current study include the use of C57BL/6J mice that exhibited raised HDL-C relative to LDL-C; this limitation was largely offset by the ability to isolate significant amounts of HDL for functional analysis and susceptibility of C57BL/6J mice to weight gain. A further limitation is the use of NaS from outset of the study — future studies interrogating the potential of NaS to attenuate established metabolic inflammation in both humans and pre-clinical studies are warranted. Finally, it is notable that potential beneficial effects of NaS on incretins during GTTs may not have been captured due to intraperitoneal delivery of glucose, as opposed to oral delivery. It will be imperative that findings pertaining to impaired RCT are investigated in human patients and this is an important future direction of this work.

In summary, we demonstrate that NaS attenuates HFD-induced IL-1β-secretion from adipose SVF, improves glucose homeostasis, prevents hepatosteatosis, and preserves HDL-CEC, all significantly improving the cardiometabolic health. Our findings indicate that the protective effects of NaS on metabolism are likely attributable to reprogramming of hepatic protein pathways to enhance fatty acid utilization in the setting of nutritional overabundance but protection against steatosis was not sufficient to prevent HFD-induced hypercholesterolemia or preserve hepatic cholesterol transporter expression.

AUTHOR CONTRIBUTIONS

Sarina Kajani: Conceptualization, Methodology, Writing. Sean Curley: Data curation and editing. Marcella E. O'Reilly: Data curation and editing. Eugene T Dillon: Data curation and methodology. Xiaofei Yin: Data curation. Weili Guo: Data curation. Kanishka N. Nilaweera: Data Curation. Lorraine Brennan: Data curation and Methodology. Helen M. Roche: Conceptualization and writing — review and editing. Fiona C. McGillicuddy: Conceptualization, Writing — Review & Editing, Methodology, Supervision, Project administration, and Funding acquisition.

FUNDING SOURCE

This research was jointly funded by Science Foundation Ireland (SFI), the Health Research Board (HRB), and the Wellcome Trust (Grant Number: 097311/Z/11/Z to FMcG) under the SFI-HRB-Wellcome Trust Biomedical Research Partnership. The lipidomics work was supported by The Comprehensive Molecular Analytical Platform (CMAP) grant under The SFI Research Infrastructure Programme, reference 18/RI/5702.

CONFLICT OF INTEREST

None declared.

APPENDIX A. SUPPLEMENTARY DATA

Supplementary data to this article can be found online at https://doi.org/10.1016/j.molmet.2021.101425.

REFERENCES

[1] Gregor, M.F., Hotamisligil, G.S., 2011. Inflammatory mechanisms in obesity. Annual Review of Immunology 29:415—445.
[2] Hotamisligil, G.S., 2006. Inflammation and metabolic disorders. Nature 444(7121):860—867.
[3] Kahn, S.E., Hull, R.L., Utzschneider, K.M., 2006. Mechanisms linking obesity to insulin resistance and type 2 diabetes. Nature 444(7121):840—846.
[4] Fazel, Y., Koenig, A.B., Sayiner, M., Goodman, Z.D., Younossi, Z.M., 2016. Epidemiology and natural history of non-alcoholic fatty liver disease. Metabolism 65(8):1017—1025.
[5] Hubert, H.B., Feinleib, M., McNamara, P.M., Castelli, W.P., 1983. Obesity as an independent risk factor for cardiovascular disease: a 26-year follow-up of participants in the Framingham Heart Study. Circulation 67(5):968—977.
[6] Rader, D.J., 2003. Regulation of reverse cholesterol transport and clinical implications. The American Journal of Cardiology 92(4A):42J—49J.
[7] Moore, R.E., Navab, M., Millar, J.S., Zimetti, F., Hama, S., Rothblat, G.H., et al., 2005. Increased atherosclerosis in mice lacking apolipoprotein A-I attributable to both impaired reverse cholesterol transport and increased inflammation. Circulation Research 97(8):763—771.
[8] Rohatgi, A., Khera, A., Berry, J.D., Givens, E.G., Ayers, C.R., Wedin, K.E., et al., 2014. HDL cholesterol efflux capacity and incident cardiovascular events. New England Journal of Medicine 371(25):2383—2393.
[9] O'Reilly, M., Dillon, E., Guo, W., Finucane, O., McMorrow, A., Murphy, A., et al., 2016. High-density lipoprotein proteomic composition, and not efflux capacity, reflects differential modulation of reverse cholesterol transport by saturated and monounsaturated fat diets. Circulation 133(19):1838—1850.
[10] McGillicuddy, F.C., de la Llera Moya, M., Hinkle, C.C., Joshi, M.R., Chiquoine, E.H., Billheimer, J.T., et al., 2009. Inflammation impairs reverse cholesterol transport in vivo. Circulation 119(8):1135—1145.
[11] de la Llera Moya, M., McGillicuddy, F.C., Hinkle, C.C., Byrne, M., Joshi, M.R., Nguyen, V., et al., 2012. Inflammation modulates human HDL composition and function in vivo. Atherosclerosis 222(2):390—394.
[12] Ralston, J.C., Lyons, C.L., Kennedy, E.B., Kirwan, A.M., Roche, H.M., 2017. Fatty acids and NLRP3 inflammasome-mediated inflammation in metabolic tissues. Annual Review of Nutrition 37:77—102.

[13] Nishimura, S., Manabe, I., Nagasaki, M., Eto, K., Yamashita, H., Ohsugi, M., et al., 2009. CD8+ effector T cells contribute to macrophage recruitment and adipose tissue inflammation in obesity. Nature Medicine 15(8):914–920.
[14] Vandanmagsar, B., Youm, Y.H., Ravussin, A., Galgani, J.E., Stadler, K., Mynatt, R.L., et al., 2011. The NLRP3 inflammasome instigates obesity-induced inflammation and insulin resistance. Nature Medicine 17(2):179–188.
[15] Reynolds, C.M., McGillicuddy, F.C., Harford, K.A., Finucane, O.M., Mills, K.H., Roche, H.M., 2012. Dietary saturated fatty acids prime the NLRP3 inflammasome via TLR4 in dendritic cells-implications for diet-induced insulin resistance. Molecular Nutrition & Food Research 56(8):1212–1222.
[16] Finucane, O.M., Lyons, C.L., Murphy, A.M., Reynolds, C.M., Klinger, R., Healy, N.P., et al., 2015. Monounsaturated fatty acid-enriched high-fat diets impede adipose NLRP3 inflammasome-mediated IL-1beta secretion and insulin resistance despite obesity. Diabetes 64(6):2116–2128.
[17] McGillicuddy, F.C., Harford, K.A., Reynolds, C.M., Oliver, E., Claessens, M., Mills, K.H., et al., 2011. Lack of interleukin-1 receptor I (IL-1RI) protects mice from high-fat diet-induced adipose tissue inflammation coincident with improved glucose homeostasis. Diabetes 60(6):1688–1698.
[18] Williamson, R.T., 1901. On the treatment of glycosuria and diabetes mellitus with sodium salicylate. British Medical Journal 1(2100):760–762.
[19] Yuan, M., Konstantopoulos, N., Lee, J., Hansen, L., Li, Z.W., Karin, M., et al., 2001. Reversal of obesity- and diet-induced insulin resistance with salicylates or targeted disruption of Ikkbeta. Science 293(5535):1673–1677.
[20] Kim, J.K., Kim, Y.J., Fillmore, J.J., Chen, Y., Moore, I., Lee, J., et al., 2001. Prevention of fat-induced insulin resistance by salicylate. Journal of Clinical Investigation 108(3):437–446.
[21] Kopp, E., Ghosh, S., 1994. Inhibition of NF-kappa B by sodium salicylate and aspirin. Science 265(5174):956–959.
[22] Yin, M.J., Yamamoto, Y., Gaynor, R.B., 1998. The anti-inflammatory agents aspirin and salicylate inhibit the activity of I(kappa)B kinase-beta. Nature 396(6706):77–80.
[23] Xu, X.M., Sansores-Garcia, L., Chen, X.M., Matijevic-Aleksic, N., Du, M., Wu, K.K., 1999. Suppression of inducible cyclooxygenase 2 gene transcription by aspirin and sodium salicylate. Proceedings of the National Academy of Sciences of the United States of America 96(9):5292–5297.
[24] Demetz, E., Schroll, A., Auer, K., Heim, C., Patsch, J.R., Eller, P., et al., 2014. The arachidonic acid metabolome serves as a conserved regulator of cholesterol metabolism. Cell Metabolism 20(5):787–798.
[25] Mitchell, J.A., Saunders, M., Barnes, P.J., Newton, R., Belvisi, M.G., 1997. Sodium salicylate inhibits cyclo-oxygenase-2 activity independently of transcription factor (nuclear factor kappaB) activation: role of arachidonic acid. Molecular Pharmacology 51(6):907–912.
[26] Hawley, S.A., Fullerton, M.D., Ross, F.A., Schertzer, J.D., Chevtzoff, C., Walker, K.J., et al., 2012. The ancient drug salicylate directly activates AMP-activated protein kinase. Science 336(6083):918–922.
[27] van Dam, A.D., Nahon, K.J., Kooijman, S., van den Berg, S.M., Kanhai, A.A., Kikuchi, T., et al., 2015. Salsalate activates brown adipose tissue in mice. Diabetes 64(5):1544–1554.
[28] Zhang, Y., Zanotti, I., Reilly, M.P., Glick, J.M., Rothblat, G.H., Rader, D.J., 2003. Overexpression of apolipoprotein A-I promotes reverse transport of cholesterol from macrophages to feces in vivo. Circulation 108(6):661–663.
[29] Shukla, S.K., Liu, W., Sikder, K., Addya, S., Sarkar, A., Wei, Y., et al., 2017. HMGCS2 is a key ketogenic enzyme potentially involved in type 1 diabetes with high cardiovascular risk. Scientific Reports 7(1):4590.
[30] Lagathu, C., Yvan-Charvet, L., Bastard, J.P., Maachi, M., Quignard-Boulange, A., Capeau, J., et al., 2006. Long-term treatment with interleukin-1beta induces insulin resistance in murine and human adipocytes. Diabetologia 49(9):2162–2173.
[31] Duval, C., Thissen, U., Keshtkar, S., Accart, B., Stienstra, R., Boekschoten, M.V., et al., 2010. Adipose tissue dysfunction signals progression of hepatic steatosis towards nonalcoholic steatohepatitis in C57BL/6 mice. Diabetes 59(12):3181–3191.
[32] Goldfine, A.B., Fonseca, V., Jablonski, K.A., Chen, Y.D., Tipton, L., Staten, M.A., et al., 2013. Salicylate (salsalate) in patients with type 2 diabetes: a randomized trial. Annals of Internal Medicine 159(1):1–12.
[33] Hauser, T.H., Salastekar, N., Schaefer, E.J., Desai, T., Goldfine, H.L., Fowler, K.M., et al., 2016. Effect of targeting inflammation with salsalate: the TINSAL-CVD randomized clinical trial on progression of coronary plaque in overweight and obese patients using statins. JAMA Cardiology 1(4):413–423.
[34] Liang, W., Verschuren, L., Mulder, P., van der Hoorn, J.W., Verheij, J., van Dam, A.D., et al., 2015. Salsalate attenuates diet induced non-alcoholic steatohepatitis in mice by decreasing lipogenic and inflammatory processes. British Journal of Pharmacology 172(22):5293–5305.
[35] Smith, B.K., Ford, R.J., Desjardins, E.M., Green, A.E., Hughes, M.C., Houde, V.P., et al., 2016. Salsalate (salicylate) uncouples mitochondria, improves glucose homeostasis, and reduces liver lipids independent of AMPK-beta1. Diabetes 65(11):3352–3361.
[36] Kersten, S., 2001. Mechanisms of nutritional and hormonal regulation of lipogenesis. EMBO Reports 2(4):282–286.
[37] Park, H., Kaushik, V.K., Constant, S., Prentki, M., Przybytkowski, E., Ruderman, N.B., et al., 2002. Coordinate regulation of malonyl-CoA decarboxylase, sn-glycerol-3-phosphate acyltransferase, and acetyl-CoA carboxylase by AMP-activated protein kinase in rat tissues in response to exercise. Journal of Biological Chemistry 277(36):32571–32577.
[38] Kim, S.H., Liu, A., Ariel, D., Abbasi, F., Lamendola, C., Grove, K., et al., 2014. Effect of salsalate on insulin action, secretion, and clearance in nondiabetic, insulin-resistant individuals: a randomized, placebo-controlled study. Diabetes Care 37(7):1944–1950.
[39] Faghihimani, E., Aminorroaya, A., Rezvanian, H., Adibi, P., Ismail-Beigi, F., Amini, M., 2013. Salsalate improves glycemic control in patients with newly diagnosed type 2 diabetes. Acta Diabetologica 50(4):537–543.
[40] Hofmann, M.A., Drury, S., Fu, C., Qu, W., Taguchi, A., Lu, Y., et al., 1999. RAGE mediates a novel proinflammatory axis: a central cell surface receptor for S100/calgranulin polypeptides. Cell 97(7):889–901.
[41] Mukai, K., Miyagi, T., Nishio, K., Yokoyama, Y., Yoshioka, T., Saito, Y., et al., 2016. S100A8 production in CXCR2-expressing CD11b+Gr-1high cells aggravates hepatitis in mice fed a high-fat and high-cholesterol diet. The Journal of Immunology 196(1):395–406.
[42] Repa, J.J., Berge, K.E., Pomajzl, C., Richardson, J.A., Hobbs, H., Mangelsdorf, D.J., 2002. Regulation of ATP-binding cassette sterol transporters ABCG5 and ABCG8 by the liver X receptors alpha and beta. Journal of Biological Chemistry 277(21):18793–18800.
[43] Janowski, B.A., Willy, P.J., Devi, T.R., Falck, J.R., Mangelsdorf, D.J., 1996. An oxysterol signalling pathway mediated by the nuclear receptor LXR alpha. Nature 383(6602):728–731.
[44] Back, S.S., Kim, J., Choi, D., Lee, E.S., Choi, S.Y., Han, K., 2013. Cooperative transcriptional activation of ATP-binding cassette sterol transporters ABCG5 and ABCG8 genes by nuclear receptors including Liver-X-Receptor. BMB Reports 46(6):322–327.
[45] Dawson, M.I., Xia, Z., 2012. The retinoid X receptors and their ligands. Biochimica et Biophysica Acta 1821(1):21–56.
[46] Chan, J., Vandeberg, J.L., 2012. Hepatobiliary transport in health and disease. Clinical Lipidology 7(2):189–202.
[47] Ananthanarayanan, M., Balasubramanian, N., Makishima, M., Mangelsdorf, D.J., Suchy, F.J., 2001. Human bile salt export pump promoter is transactivated by the farnesoid X receptor/bile acid receptor. Journal of Biological Chemistry 276(31):28857–28865.

